LANGMUIR

Multivalent Patchy Colloids for Quantitative 3D Self-Assembly Studies

Marlous Kamp,* Bart de Nijs, Marjolein N. van der Linden, Isja de Feijter, Merel J. Lefferts, Antonio Aloi, Jack Griffiths, Jeremy J. Baumberg, Ilja K. Voets, and Alfons van Blaaderen*

Read Online

| ACCESS | | Metrics & More | | Article Recommendations | | Supporting Information |

ABSTRACT: We report methods to synthesize sub-micron- and micron-sized patchy silica particles with fluorescently labeled hemispherical titania protrusions, as well as routes to efficiently characterize these particles and self-assemble these particles into non-close-packed structures. The synthesis methods expand upon earlier work in the literature, in which silica particles packed in a colloidal crystal were surface-patterned with a silane coupling agent. Here, hemispherical amorphous titania protrusions were successfully labeled with fluorescent dyes, allowing for imaging by confocal microscopy and super-resolution techniques. Confocal microscopy was exploited to experimentally determine the numbers of protrusions per particle over large numbers of particles for good statistical significance, and these distributions were compared to simulations predicting the number of patches as a function of core particle polydispersity and maximum separation between the particle surfaces. We self-assembled these patchy particles into open percolating gel networks by exploiting solvophobic attractions between the protrusions.
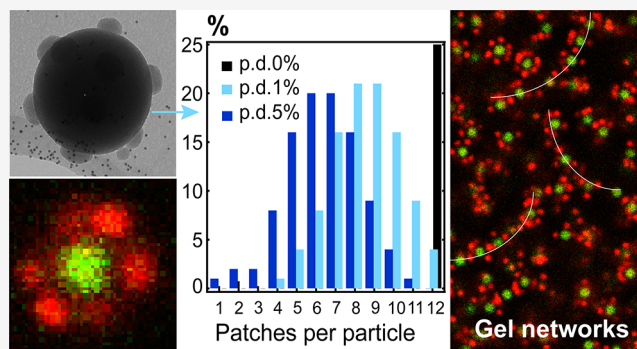
INTRODUCTION

Patchy particles are colloidal particles with site-specific directional interactions,[1-3] and when subjected to Brownian motion, they are model particles analogous to atoms with a valency[4] on a scale which is accessible to optical microscopy techniques. Patchy colloids have seen a steep rise in interest in the past decade[5-26] on account of their potential to form new types of bonds[4,27] and phases.[2,28-41] Until ~5 years ago, experimental realization of patchy particles and in particular of their predicted phases lagged far behind theoretical descriptions; however, recently experimental systems have started to catch up with theory and computer simulations. First, the lag was due to the difficulty of synthesizing particles with multiple well-ordered patches (i.e., multivalent particles). Few synthetic methods allow modification of colloids site-specifically, especially in bulk. Most recent experimental systems presented are in fact still limited to Janus spheres, dumbbells and rods,[27,42-45] and two-patch systems,[29] which can nevertheless result in very rich phase behavior. A different strategy that can be used to create rich phase behavior is mixing patchy and nonpatchy particles or mixing various types of patchy particles.[16,46] A few beautiful systems with multiple patches have now been introduced.[47-53] Particle polydispersity, which is the variability in size and shape of particles and patches, also decreases the extent to which theory and experiments can be compared. Second, experiments lagged behind theory due to

the difficulties in creating the required interaction strengths and depths to create the desired selectivity.[54] In the past five years, however, patch–patch interactions have been created through mechanisms as diverse as DNA interactions,[14,18,49] supramolecular chemistry,[14,55,56] solvophobic interactions,[29,57] wetting-induced forces,[58] surface–liquid capillary bridging,[59] and click reactions.[60] The studies referenced taken together demonstrate important progress in recent years in the synthesis of patchy particles and the interparticle interactions required to create new phases.

A practical difficulty in studying multivalent patchy particles is that, to accurately study such systems by imaging techniques in real time, in 3D, and *in situ*, it is essential to be able to distinguish the core and the patches in the imaging technique used. Many details that would be available from a quantitative real space analysis and would allow direct comparison with theory and simulations would not be available through the use of scattering techniques. This point is rather underexposed in the struggle to synthesize monodisperse systems with the
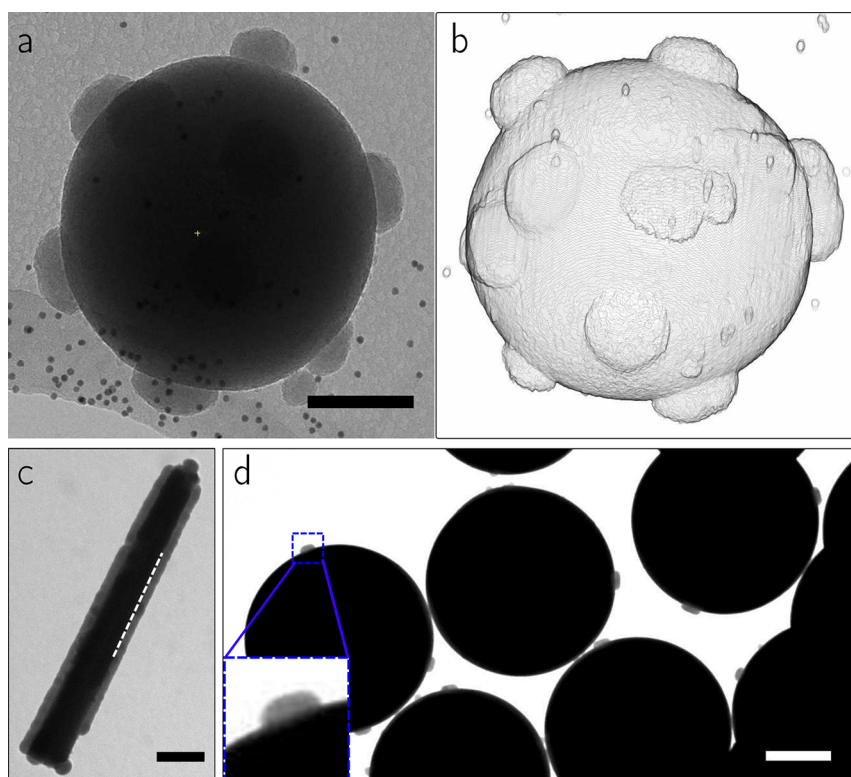
Figure 1. Typical transmission electron microscopy (TEM) micrographs of silica particles with silica protrusions fabricated by the annealing method with a silane coupling agent [3-methacryloxypropyltrimethoxysilane (MPTMS)] patterning[47] for sub-micron-sized and micron-sized core particle sizes. (a) Silica protrusions on a submicron silica particle (average particle size 411 ± 4 nm, polydispersity 4%). The black dots are gold markers for the tomographic reconstruction. (b) Surface rendering of a tomographic reconstruction of the particle in panel a obtained via electron tomography. (c) TEM micrograph of a fluted rod with 6 protrusions. The dotted line serves as a guide to the eye for the edge of one of the protrusions. (d) Silica protrusions on micron-sized silica particles (1.43 ± 0.02 μm, polydispersity 2%). The annealing temperature during synthesis was 500 °C (10 h) for this sample. Scale bars denote (a) 100 nm, (c) 300 nm, and (d) 500 nm.

desired interaction strengths and will be addressed in the current work.

Even with the progress in experimental realization of patchy particles, there are still unexplored or underexplored predictions and aspects first introduced by theoretical calculations and simulations studies, such as the behavior of patchy particles at low volume fractions,[28,61] out-of-equilibrium,[62,63] and on substrates.[64−67] In this work we focus on particles with high coordination numbers of up to 12 patches, which are also regularly placed, reflecting neighboring particles inside a colloidal crystal. Several recent theoretical studies have addressed self-assembly of patchy particles with high coordination numbers. For example, Reinhardt et al. found that these can form regular/crystalline structures through patch−patch interactions; however, the free-energy barrier to nucleation is considerably higher than for, e.g., tetrahedral particles, requiring higher supersaturation.[68] Newton et al. demonstrated that patchy particles with a higher valency but weaker interactions form structures with fewer defects than particles with a lower valency and stronger interactions.[69] Moreover, a number of theoretical studies have shown that patchy particles of intermediate and high valency can form low-density gel networks.[25,28,70−73] Such systems were observed experimentally in clay particle dispersions,[74] and we will touch upon the creation of such systems in this work as well. Another concept that was initially introduced in a theoretical paper is that of inverse patchy particles (IPCs),[15,75−77] where patches adhere to the antipatch of

other patchy particles. Experimental examples of IPCs have recently been presented by van Oostrum et al.[78] and Sabapathy et al.[79]

In this paper, we describe the development of a system of multivalent patchy particles with distinguishable fluorescently labeled cores and protrusions, the large-scale quantitative characterization and analysis of these systems using confocal microscopy, as well as the self-assembly of these patchy particles into gel structures. Our synthesis methods extend upon earlier work by Wang et al.[47] and by Bae et al.,[48] who grew, respectively, (nonlabeled) silica and titania protrusions onto silica colloids. In the methodologies developed by these groups, use was made of the fact that, for touching particles in, e.g., a packing of ball bearings, the coordination numbers and local symmetries can be determined by poring a paint in and letting this dry, a method followed by Bernal and others many decades ago.[80] The reason being that the dried paint could not reach into the regions where particles touched or were very close to touching (the diameter of the rings formed were even a measure of how close the particles were). In the procedure we used, the paint is replaced by a silane coupling agent that can coat the silica surface exposed, but not where particles are touching each other. We used crystalline packings of the silica colloids; however, clearly the method can immediately be applied to create less regular patch distributions if we instead had used glasses, where the number of neighbors is almost the same as that in close-packed crystals.[81] After the coating reaction, the silica particles in the close-packed colloidal
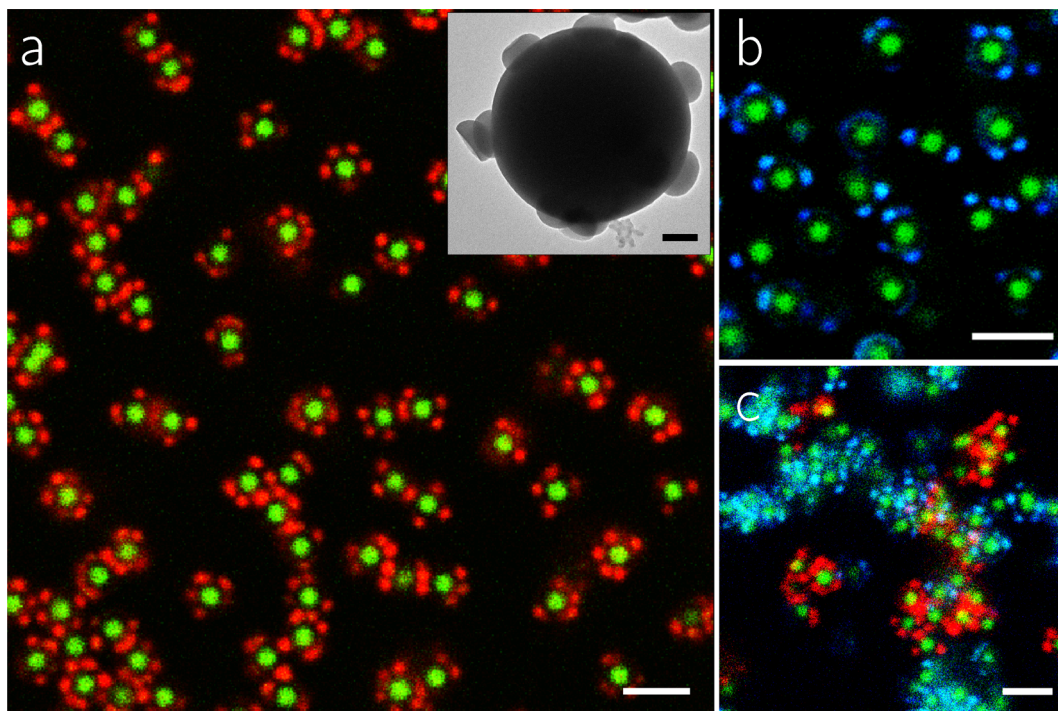
Figure 2. Patchy silica particles with dye-labeled titania protrusions fabricated by the anhydrous method with an octadecyltrimethoxysilane (OTMS) patterning. (a) Confocal micrograph of OTMS-patterned silica particles (core particle size 1085 ± 5 nm in ethanol (SLS)) with an FITC-labeled core (depicted in green) and RITC-labeled titania protrusions (depicted in red) in cyclohexyl chloride (CHC). Inset: TEM micrograph of one such particle. (b) Confocal micrograph of OTMS-patterned silica particles with an FITC-labeled core (depicted in green) and DEAC-SE-labeled titania protrusions (depicted in blue) in CHC. (c) Confocal micrograph of mixture of the particles used in panels a and b. The scale bars denote 2 μm and (inset) 200 nm.

crystals can still be redispersed as single particles if enough energy is used, for instance, by sonication and if the size is larger than several hundred nm such that shear can create strong enough forces. Already the redispersed system is composed of patchy colloids as the bare and silane coupling agent covered surfaces have different properties, like surface tension and charge density. It has been shown that, by the right choice of silane coupling agent, both extra silica and/or titania can be deposited specifically onto the bare silica patches forming patches with also a geometric component to the patchiness. We demonstrate how confocal microscopy, using the fluorescent labeling of cores and patches, can be harnessed to quantitatively analyze the numbers of patches per particle for large numbers of patchy particles. As we expected the number of patches to be strongly affected by polydispersity, we compared our experimental results and analysis to numerical simulations; we find good agreement. Finally, with the silane modified silica core and pristine titania patches, we explored attractions caused by both van der Waals forces and opposite surface charges, in the presence of generally low ionic strengths, enabling charge repulsions to also play a role. We study the self-assembly of these patchy particles in low-polar solvents, and find that the colloids form open, percolating structures, where the dispersion medium determines the nature of the patch−patch interactions.

■ RESULTS AND DISCUSSION

Silica Protrusions on Sub-Micron- and Micron-Sized Particles. Following Wang and co-workers,[47] silica particles were chemically patterned by immersing a dried (and thus close-packed) and annealed colloidal crystal of sub-micron-

sized particles in an ethanolic reaction medium containing the silane coupling agent 3-methacryloxypropyltri-methoxysilane (MPTMS). After the colloidal crystal was redispersed as single particles by sonication, well-defined silica protrusions were grown onto these patterned colloids, with little to no silica deposition elsewhere on the colloid's surface (the "antipatch"). Typical images of the product particles are shown in Figure 1a,b. For several particles, all protrusions were visualized by means of electron tomography (ET)[82] (see Figure 1b and Videos SV1−SV3). This technique circumvents the occlusion of the bottom of the particle that occurs in scanning electron microscopy (SEM),[48] and to our knowledge ET is used here for the first time on such patchy particles. In agreement with ref 48, the number of protrusions on each particle was in general below 12 (Figures S1 and S2), the coordination number in a close-packed colloidal crystal of purely monodisperse spheres. Possible causes for this discrepancy between the maximum and the observed number of protrusions per particle are crystal defects in the colloidal crystal used for synthesis,[83] and more importantly the fact that the colloids from which these patchy particles were synthesized were not perfectly monodisperse,[48] a point which we will discuss in more detail later.

To demonstrate the versatility of the approach, we also prepared patchy rodlike silica particles in this manner. In short, rodlike particles developed in our group[84,85] were allowed to sediment and form a smectic phase, and the colloidal crystal of rods was dried, annealed, and treated with MPTMS. After redispersion of the particles, silica was grown onto the nonmodified patches, resulting in fluted rodlike particles with silica wings (Figure 1c and Section S2, Figure S3).
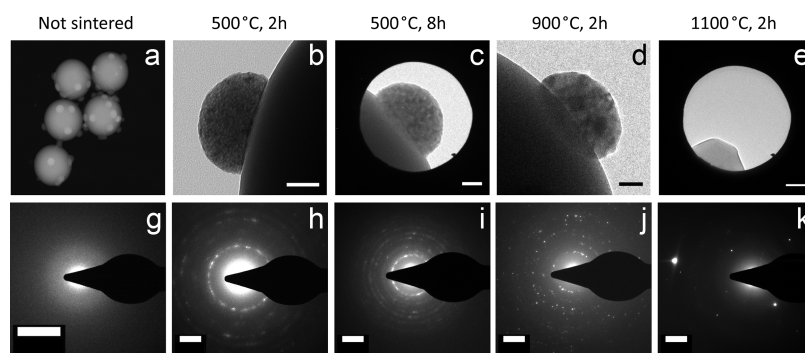
Figure 3. Crystalline titania protrusions. Close-ups (top row) and electron diffraction patterns (bottom row) of patchy particles with APTES-RITC-labeled titania protrusions annealed at various temperatures and annealing times: (a, f) No annealing; no diffraction rings or spots appear. (b, g) 2 h at 500 °C; (c, h) 8 h at 500 °C; (d, i) 2 h at 900 °C; (e, j) 2 h at 1100 °C. Scale bars denote 50 nm.

The synthesis procedure was also extended to silica core particles larger than a micron (Figure 1d and Video SV2), because larger colloids and larger patches are more suitable for quantitative 3D fluorescence microscopy studies.[81] In micron-sized particles, we observed comparatively more protrusions when the colloidal crystal was annealed at a lower annealing temperature (600 °C instead of 750 °C) (Figure S4), most likely because there is less shrinkage of the particles at these reduced temperatures.[86−88] In further experiments we used an "anhydrous" synthesis route (see the Methods section) that avoids annealing by using an apolar solvent as the reaction medium for surface functionalization of the colloidal crystal (since colloidal silica crystals were found to redisperse too easily upon immersion in more polar solvents). This anhydrous synthesis route avoided particle shrinkage and this observed variability, while in addition enabling fluorescently labeled silica particles to remain fluorescent.

Fluorescently Labeled Silica Protrusions. Van Blaaderen and Vrij incorporated a fluorescent dye derivative (fluorescein isothiocyanate, FITC) into spherical silica particles by covalently coupling the dye to the silane coupling agent (SCA) 3-aminopropyltriethoxysilane (APTES), and allowing the conjugate to cocondense with the silica precursor.[89] FITC was incorporated selectively into silica protrusions using this method (Section S3, Figure S5). Initially, however, the APTES-FITC conjugate facilitated silica growth on the antipatch, which was coated with MPTMS, most likely due to the positively charged amine group adsorbing also to the negatively charged antipatch. This excess silica growth reduced when the MPTMS grafting step was performed twice, and the protrusions became well-defined. Nevertheless, a monolayer of attached FITC dye was still visible as a ring around the particles. This same issue occurred for an MPTMS grafting applied via the anhydrous route. A surface-patterning of SCA octadecyltrimethoxysilane (OTMS) instead of MPTMS, applied via the anhydrous route, did produce acceptable patch shapes and successfully prevented binding of APTES−dye conjugates, showing that OTMS molecules provide sufficient steric hindrance to shield the silica surface from dye−APTES conjugates forming siloxane bonds with the SCA coated surface. Surface-patterning with OTMS has the additional advantage that it creates a larger difference in hydrophobicity between the patch and the antipatch, increasing the chemical patchiness. However, the dispersibility of OTMS-grafted particles in ethanol was low, and undesirable particle clustering takes place in the Stöber-like reaction

mixture during protrusion growth, possibly affecting the protrusion shapes. Therefore, the dye-labeling method was further optimized as described below, by infiltrating titania protrusions with dye−SCA conjugate.

Fluorescently Labeled Amorphous Titania Protrusions. Amorphous titania protrusions were grown onto MPTMS- and OTMS-patterned silica particles by hydrolysis and condensation of the titania precursor titanium IV butoxide (TBT).[48] In contrast to Bae and co-workers,[48] we did not observe a deterioration of the titania protrusion shape due to magnetic stirring. Occasionally, loose hemispherical protrusions were encountered in TEM images (see Figure 2a, inset), most likely dislodged due to internal stresses caused by heating and/or densification by the electron beam.[90,91] Such an effect was previously observed by Demirörs et al. in silica−titania core−shell particles, where the titania core became movable upon annealing.[92] These amorphous titania protrusions were successfully labeled *postsynthesis*, aided by the high micro-porosity of the amorphous and not fully condensed titania,[92] by infiltration with APTES−dye conjugate resulting in a covalent attachment of the dye rhodamine isothiocyanate (RITC) to the titania. These patchy particles were imaged *in situ* by confocal microscopy, where protrusions and cores were clearly distinguishable (Figure 2a).

For future in-depth studies on the phase behavior (e.g., gelation, see also the Self-Assembly of Patchy Particles via Solvophobic Interactions section for more detail) of the patchy particles, it is interesting to have different dyes correspond to a specific type of surface ligand on the protrusion. The UV-excitable fluorescent dye 7-diethylaminocoumarin-3-carboxylic acid succinimidyl ester (DEAC-SE) was also incorporated into the titania protrusions (Figure 2c). Trau et al. studied this dye previously at a silica surface.[93] DEAC-SE is amino-reactive and therefore was covalently linked to titania in the same way as the isothiocyanates FITC and RITC, i.e., via coupling to APTES and infiltration *postsynthesis*. With DEAC-SE emitting in the blue, these three dyes taken together allow the study of mixtures of patchy particles (Figure 2c).

Next, we investigated whether the protrusions of the patchy particles could be characterized *in situ* by the super-resolution microscopy techniques stimulated emission depletion (STED) and photoactivated localization spectroscopy (PALM). A dye for PALM was selectively attached to the protrusions[94,95] (see Section S5 (Figure S7)). However, the improvement in resolution was modest compared to conventional confocal microscopy (Figure S6) as the silica core and titania
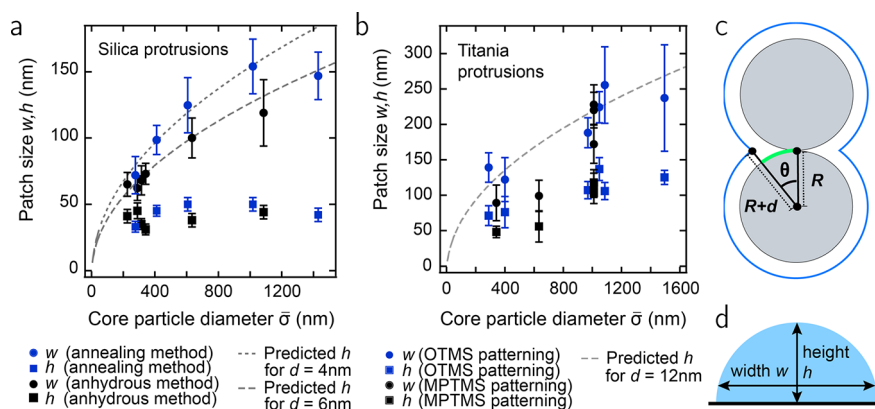
Figure 4. Protrusion dimensions: widths and heights. (a) Average patch widths w (circles) and heights h (squares) as a function of core particle diameter $\bar{\sigma}$ for patchy particles grown via the annealing method (blue) and via the anhydrous method (black). The patch sizes of the "annealed" (blue) series are plotted against the particle diameter as measured after annealing, which is responsible for the slight offset in $\bar{\sigma}$. Error bars for the average particle diameter are generally smaller than the symbol size. Error bars in the vertical direction are standard deviations of the patch size measurements, i.e., a "polydispersity" in the patch size. Dashed lines are fits to eq 1 for $d = 4$ nm and $d = 6$ nm. (b) Average patch size of titania protrusions[48] as a function of $\bar{\sigma}$. Blue symbols indicate an OTMS patterning and black symbols an MPTMS patterning. The dashed line is a fit to eq 1 for $d = 12$ nm. (c) Schematic indicating the parameters used to predict protrusion widths. R is the particle radius, d is the size of the grafting molecule, and θ is opening angle of the patch. (d) Schematic indicating how patch width w and patch heights h were measured.

protrusions vary considerably in refractive index ($n = 1.45$ vs $n = 1.55$[96]) such that these patchy particles cannot be completely index-matched. In future studies, it is therefore interesting to prepare all-titania patchy particles with a titania core and protrusions to benefit from increased resolution from STED or PALM.

Crystalline Titania Protrusions. For potential use in catalysis[97] or active matter,[23,97,98] it is of interest to convert the amorphous titania protrusions into crystalline polymorphs, as can be achieved by annealing. Nonlabeled titania protrusions (Figure S8) deformed in this process (Figure S9a). In contrast, particles with titania protrusions that had been infiltrated with APTES-RITC were successfully annealed without any distortion of the protrusions (2 h at 500 °C, Figure S9b). This difference in structural integrity is a result of the APTES forming an organosilica scaffolding inside the titania mesoporous structure, cf. Demirörs et al., who observed that spherical amorphous and not fully condensed titania particles decrease as much as 40% in diameter at 650 °C due to the collapse of the porous structure,[92] while titania spheres infiltrated with silica shrink considerably less.[96]

To examine the crystallinity of the annealed dye-labeled titania protrusions, selected area electron diffraction (SAED) was performed (Figure 3). Protrusions annealed at 500 °C diffracted the electron beam into rings, indicating the presence of a form of polycrystalline titania. Apparently, the silica does not intervene chemically at these temperatures and remains dispersed independently in between the crystallites, as already noted in ref 96. Annealing for 8 h instead of 2 h at 500 °C produced slightly more pronounced rings. Protrusions annealed at 900 °C displayed diffraction spots rather than rings, indicating that these consisted of fewer crystalline domains with respect to the 274 nm area used to obtain the diffraction pattern. Annealing at 1100 °C produced diffraction spots only; this titania is predominantly monocrystalline. In short, higher annealing temperatures increase monocrystallinity in these titania protrusions, more so than longer annealing times do.

The electron diffraction patterns are in line with anatase titania (see Section S7), although the scarcity of diffraction

spots in the SAED pattern of particles annealed at 1100 °C prevents conclusive identification of this titania polymorph. The monocrystallinity of these protrusions nevertheless showed in their faceting (Figure 3e) and Bragg reflections in dark-field TEM (Figure S10).

Quantifying and Modeling Patch Growth Using TEM Micrographs. To quantify the protrusion growth and evaluate quantitatively the effects of particle polydispersity, protrusion widths w and heights h were measured in TEM micrographs (Figure 4). For both silica and titania protrusions, w increases as a function of average core particle diameter $\bar{\sigma}$. Note that, here, the error bars in the vertical direction denote not the measurement uncertainty but the standard deviation of w or h, that is, a polydispersity δ_w (δ_h) in the protrusion width (height). The protrusion width for particles of 411 nm with silica protrusions prepared via the annealing method ($w = 99$ nm, $\delta_w = 11$ nm) agrees well with that observed by Wang et al. for 415 nm particles ($w = 95$ nm, $\delta_w = 13$ nm).[47] Particles prepared by the annealing method[47] had larger widths w than those prepared by the anhydrous method, which conforms to expectations since sintering broadens the contact areas.

We analyze the results in a simple model for the patch formation by assuming that patches result from size exclusion of the SCA from the contact areas in the crystal (Figure 4c). In detail, the SCA molecule cannot reach the particles' surface from a location where the distance to the surface is longer than its stretched length d. The volume containing such positions around a particle of radius R is a shell of radius $R + d$. The patch is formed by the intersection of the shells (patch radius $w/2$ indicated in green), yielding a patch width w of

$$w = 2R \cos^{-1}\left(\frac{R}{R + d}\right) \tag{1}$$

Based on atom–atom bond lengths and angles[99] the maximum length of a stretched MPTMS molecule is 1.9 nm. The experimental values for silica patch widths (without sintering), however, are better described by the curves of predicted patch sizes for $d = 4$ nm (see Figure 4a). A plausible reason is that the SCA molecules form oligomers before attaching to the surface, resulting in a larger effective size d. In
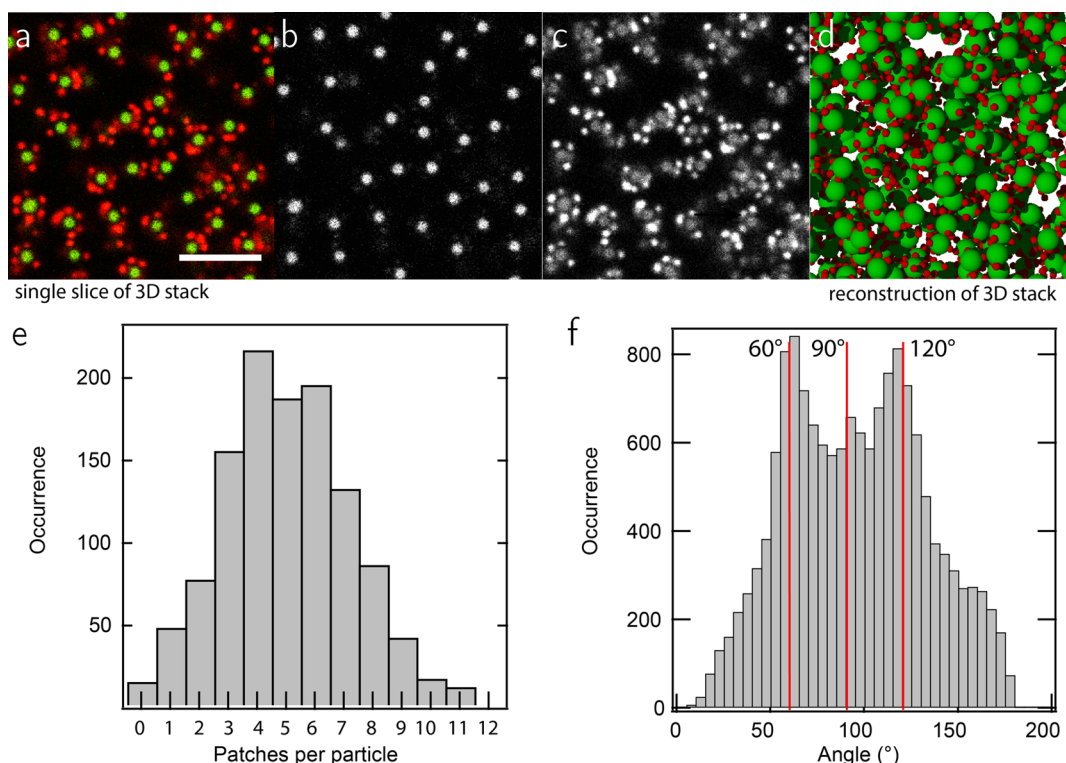
Figure 5. Tracking and particle fitting from a 3D confocal data set, and experimental patch number distributions. (a) Single slice in a 3D confocal stack of patchy silica particles with dye-labeled titania protrusions in dodecanol. Scale bar denotes 4 μm. The full stack is displayed in Video SV4. FITC-labeled cores are displayed in green and RITC-labeled protrusions in red. Same image as in panel a split by the imaging channels, resulting in (b) mostly cores and (c) only protrusions. There is a slight bleeding-through of the FITC into the RITC channel. (d) Computer-rendered reconstruction of the dispersion, obtained by smoothing, thresholding, and tracking the image frames split by channel as in panels b and c. This image displays all core particles (green) and patches (red). (e) Patch number distributions obtained from the particle tracking the dispersion of patchy particles (Figure S11). (f) Histogram of the angles between all protrusions on each particle, for the same dispersion as in panel e.

addition, surface roughness is not taken into account in this simple model. OTMS molecules (of maximum stretched length 3.3 nm) are larger than MPTMS molecules, and this explains why titania protrusion widths correlated best with an even larger effective size $d = 12$ nm (Figure 4b).

Protrusion heights h for silica patches remained nearly constant with the core particle diameter (Figure 4a), whereas an increase was expected (see Section S7 for a calculation). For titania protrusions, h did increase with particle diameter. This difference cannot be attributed to a larger amount of precursor [we added 9 μmol of tetraethylorthosilicate (TES) versus only 0.3 μmol of TBT per milligram silica particles]. We tentatively attribute this discrepancy to TES hydrolysis and condensation in base-catalyzed solutions continuing beyond the 2 h of reaction time.[100−102] Despite the addition of the TES happening over 11 h, possibly not all added TES condensed over the subsequent 2 h of reaction time.

Number Distributions of Patches/Protrusions per Particle: Theory and Experiment. The number of protrusions on a patchy particle can be determined accurately using electron tomography, as we performed in Figure 1b. However, this technique is too laborious for a large number of particles. When cores and protrusions are labeled with different dyes, confocal microscopy becomes a powerful tool to study large numbers of patchy particles. We demonstrate here that confocal microscopy can be used (1) to reconstruct dispersions of patchy particles to observe their 3D structure[81] and (2) to extract meaningful data such as the distribution of protrusions per particle and the symmetry of the patches around each core,

reflecting the local symmetry inside the colloidal crystal from which they originated.

Video SV4 shows a confocal z-stack of patchy particles (silica core particles of diameter 1085 nm and 1% polydispersity, with titania protrusions) in dodecanol ($n = 1.44$ at 20 °C, nearly matching silica), which we refer to as sample A. Figure 5a shows a single slice from this stack. The frames of the 3D stack can be split into images with only cores (Figure 5b) or only protrusions (Figure 5c) on account of the different labelings. A tracking algorithm was developed with which the positions of particle cores and protrusions within the stack were determined, and a digital directory of these positions was created. By attributing to the core and the protrusions radii $d1$ and $d2$, known from TEM measurements, a computer-rendered reconstruction of the dispersion was then obtained. The algorithm was first tested on a sparse sample of patchy particles (Figure S11a,b) and subsequently used to track and reconstruct sample A (Figure 5d, and full figure in Figure S11c).

The average number of protrusions per particle follows immediately from the number of cores and protrusions found by the tracking algorithm. For sample A, tracking revealed 1194 cores and 5994 patches, or an average patch number of 5.0. To establish how the protrusions are distributed over the core particles, each protrusion was assigned to its closest core. A cutoff distance of $1.5\overline{\sigma}/2$ for the maximum allowed distance of a protrusion to a core was also determined (Figure S11d). Subsequently, the number of protrusions was counted for each core, yielding the histogram in Figure 5e for sample A. The
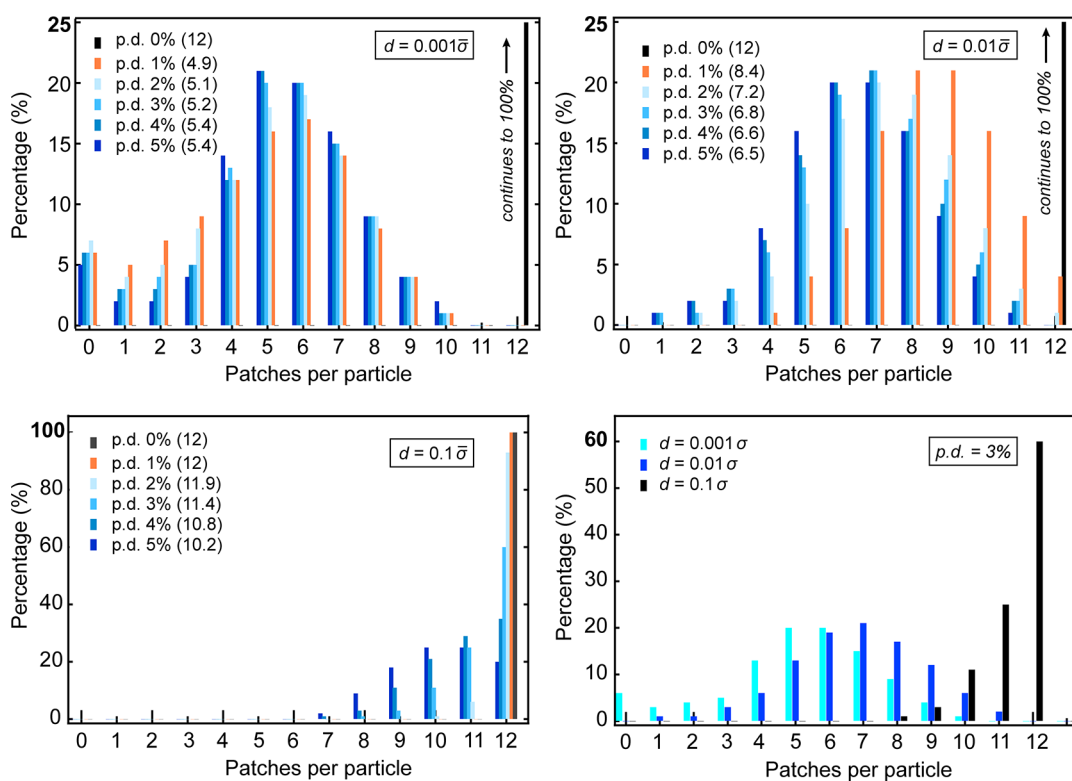
Figure 6. Patch number distributions as calculated by simulations for particles of p.d. = 0−5% and cutoff distance (a) $d = 0.001\bar{\sigma}$, (b) $d = 0.01\bar{\sigma}$, and (c) $d = 0.1\bar{\sigma}$. The vertical axis is discontinued at 25% for clarity in panels a and b. In the legends, the average number of patches per particle is indicated in brackets for each distribution. (d) Patch number distributions as calculated by NPT simulations for particles of p.d. = 3%, comparing the distributions for three different cutoff distances d.

histogram reveals a distribution centered around 5 protrusions per particle, with an fwhm of ≈2 protrusions/particle, a point we will come back to later. The angles between any two protrusions on each core particle were also extracted, yielding the histogram in Figure 5f. The distribution displays clear peaks at 60°, 90°, and 120°, which correspond well with bond angles in an FCC colloidal crystal. Most likely the colloidal crystal also contained glassy areas, since the peaks in the bond angle distribution are broad. The resolution of the distribution also does not allow the discernment of whether there is a contribution of hexagonal close-packed (HCP) order, which would be visible as additional peaks or shoulder peaks at 108° and 146°. Nevertheless, these data show that the protrusions are indeed located at the points of contact in a close-packed colloidal crystal, even though in TEM images this order is difficult to discern due to the low average number of protrusions per particle (5.0).

To further put these experimental results into perspective, patch number distributions were predicted by simulations (see the Methods section for computational details). The influence of two particle characteristics were examined: the size polydispersity of the core particle, denoted p.d., and the maximum "allowed" separation between the particle surfaces that still results in patch formation, called the cutoff distance d. Figure 6a shows simulated patch number distributions for a fixed cutoff distance of 0.1% of the average core particle diameter $\bar{\sigma}$ and varying p.d. For a purely monodisperse system, all particles possess 12 patches (black graph), as expected in a close-packed crystal. For higher p.d., the patch number distribution quickly drops to lower average patch numbers of around 5 patches per particle. This finding is in agreement with

the experimental results in Figure 5 and explains why in general the presented synthesis method will not yield "perfect" particles with 12 patches. For larger cutoff distances d, the decrease in average patch number with increasing p.d. is smaller (Figure 6a−c). This becomes even better visible in Figure 6d, where the patch number distributions are displayed for a fixed p.d. (3%) but varying d. The number of patches per particle shifts to higher values for increasing cutoff distances d, in accordance with our model in Figure 4.

We compare our experimental results to these simulations. We estimate the experimental cutoff distance for the core particles of the sample in Figure 5 to be $d = 0.003\ \bar{\sigma} − d = 0.011$ (since $\bar{\sigma} = 1085$ nm and $d = 3$ nm − 12 nm based on OTMS stretched length of 3.3 nm and the fitted $d = 12$ nm in Figure 4b). For p.d. = 1%, the simulations predict a patch number distribution centered around 6 patches per particle (with an average of 4.9) for $d = 0.001\bar{\sigma}$, and a distribution centered around 8−9 patches per particle (with an average of 8.4) for $d = 0.01\bar{\sigma}$ (Figure 6a,b). That is, the experimentally observed distribution with an average of 5.0 patches per particle is in agreement with the expected patch numbers based on the simulations, but only when the stretched length of the polymer is taken as the cutoff distance rather than their fitted effective size. An explanation for the discrepancy is that domain walls, point defects, and cracks were not taken into account in the simulations. On the experimental side, small patches (e.g., with a cross section smaller than one pixel) may not be recorded in the confocal microscope or not counted in the tracking algorithm. The possibility that some titania grows beyond the edges of the patch, hence increasing the fitted
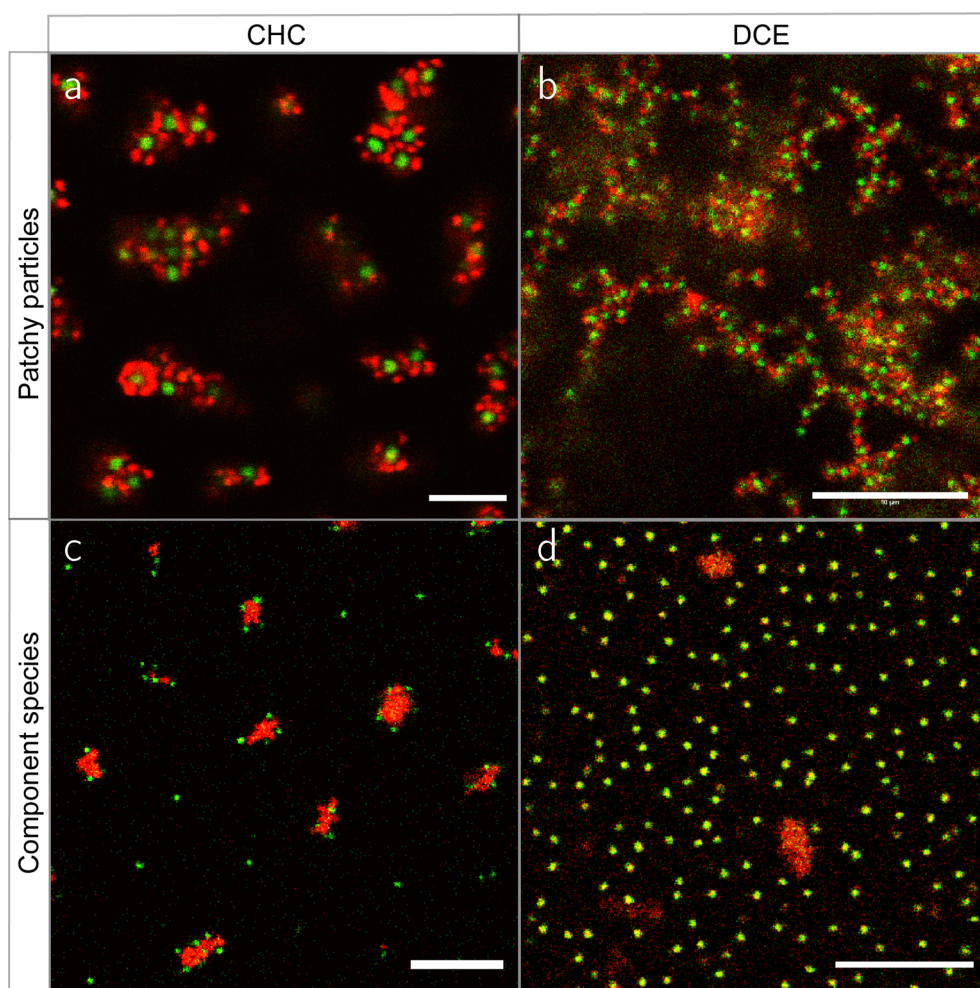
Figure 7. Patchy particles and component species in CHC and DCE. Patchy particles (silica core of 1.0 μm, with OTMS patterning and RITC-labeled titania protrusions) dispersed in (a) CHC and (b) DCE, after turning the sample upside down for confocal imaging. (c) OTMS-grafted silica and RITC-labeled titania in CHC. The surface charge was negative on the silica and positive on the titania. (d) OTMS-grafted silica and RITC-labeled titania in DCE. The surface charge was positive on both the silica and the titania. A Gaussian filter was applied to all images to reduce noise.

effective size of the grafting molecule, cannot be excluded either.

Self-Assembly of Patchy Particles via Solvophobic Interactions. Patchy silica particles with titania protrusions can potentially sustain patch−patch interactions. In low-polar media, the OTMS chains are solvated, provide steric stabilization, and in addition cause the antipatches to repel each other via a steric interaction. The titania protrusions, on the other hand, do not have a steric stabilization to counteract the van der Waals attractions among them, and this possibly creates patch−patch attractions. In addition, the particles' surfaces may carry charge from (remaining) terminal OH groups at the patches and protrusions, causing charge-related attractions or repulsions. Here, we manipulated the inter-actions between patchy particles (with titania protrusions and OTMS patterning on the antipatch) by dispersing them in cyclohexyl chloride (CHC) and 1,2-dichloroethane (DCE). The potential patch−patch interactions are based on van der Waals interactions, hence irreversible in character, and therefore these particles are expected to form gels rather than crystalline structures upon self-assembly via such interactions. Moreover, the complex colloids presented here possess a comparatively wide distribution of the number of

patches per particle; hence, even in the case of reversible interactions, gel structures would be expected for this particular system of patchy particles.

Both in CHC and in DCE, percolating open gel phases were indeed observed for these patchy particles (see Figure 7a,b and Videos SV5 and SV6). To investigate the nature of the interparticle interactions, we mixed dispersions of (nonpatchy) OTMS-grafted silica particles with dispersions of RITC-infiltrated titania particles. In deionized CHC, the OTMS-grafted silica particles formed a hexagonal long-ranged crystal[103,104] indicating a strong electrostatic repulsion, while RITC-labeled titania particles aggregated. When mixed, the silica particles adhered to the titania clusters in this medium (Figure 7c and Video SV7). This observation implies that, in dispersions of patchy particles *in CHC*, the protrusions stick to the antipatch (and likely also to other titania protrusions; that is, the particles behave only partially as "inverse patchy particles"[15,75−77]). In DCE, on the other hand, the titania particles also formed large aggregates, but the two types of particles did not adhere to each other (Figure 7d and Video SV8). It is therefore likely that *in DCE* the protrusions adhere exclusively to other protrusions: a patch−patch interaction.

To gain further insight into the charge interactions in the systems, the electrophoretic mobility of titania particles and OTMS-grafted silica particles was measured in both these low-polar media using laser Doppler electrophoresis. Since RITC absorbs the laser wavelength (633 nm), nonlabeled titania was used as an indication of the sign and order of magnitude of the charge. While the titania particles were positively charged in both DCE and CHC, the OTMS-silica particles were negatively charged in CHC and positively charged in DCE (Section S9, Figure S12). Therefore, it is likely that *in CHC* the (positively charged) titania protrusions stick to the (negatively charged) OTMS-silica cores. In contrast, *in DCE* all constituents are positively charged, and since the particles form a network, most likely the titania protrusions adhere to other protrusions. Such a patch−patch attraction could have a partially solvophobic character given the absence of alkane chains, and van der Waals attraction will certainly also contribute given the dielectric constant mismatch.

The gel structure in DCE (as well as the one in dodecanol, Video SV4 and Figure S13) illustrates the prediction by Bianchi et al. in ref 28: "it is foreseeable that, with small $\langle M \rangle$ patchy particles," (here $\langle M \rangle$ = 5.0) "disordered states in which particles are interconnected in a persistent gel network can be reached at low T without encountering phase separation."

■ SUMMARY

We prepared patchy particles with silica and titania protrusions by extending upon the works of Wang et al.[47] and Bae et al.[48] For the case of silica protrusions, we made the following advancements. Through an anhydrous grafting method of the silane coupling agents used to cover the exposed silica surfaces, we were able to eliminate the need for a temperature-induced annealing step in the synthesis route. A fluorescent dye was incorporated into the protrusions via the method of van Blaaderen et al.,[89] for which it was important to use a patterning of the silane coupling agent OTMS to cover free silica surfaces and to prevent binding of the dye conjugate to the antipatch. Electron micrographs were used to examine how the size of the protrusions depends on core particle size and synthesis route. A simple model was used to estimate how the diameter of the protrusions was dependent on the core particle diameter in a way consistent with size exclusion of (oligomers of) the grafting molecule from the contact areas. We also extended the synthesis method to silica rods, which resulted in fluted rodlike particles with up to six wing-shaped protrusions along the length of the rods.

The following advancements were made for the case of titania protrusions. Titania protrusions were covalently labeled *postsynthesis* with various fluorescent dyes (FITC, RITC, and DEAC-SE) by infiltration of the porous titania with dye−APTES conjugate, rendering the particles suitable for confocal microscopy. DEAC-SE is a blue-emitting dye which was used for the first time here to label colloidal particles for confocal microscopy. The protrusions were also successfully labeled with the rhodamine derivative Cage 552 and imaged by the super-resolution technique PALM. True nanoscopy resolutions as obtainable through STED confocal microscopy were not achieved, most likely because of the negative effect of the scattering titania patches on the point spread function.

Patchy particles with titania protrusions infiltrated with rhodamine-APTES were annealed at temperatures up to 900 °C, which converted the protrusions to anatase titania (most likely within a silica matrix) with excellent preservation of the

protrusion shapes. The domain sizes of crystallites increased with annealing time and temperature. These findings are potentially useful for catalytic processes and self-propelling particles.

We performed simulations in which randomly distributed polydisperse particles on face-centered cubic colloidal crystal lattices were compressed, to simulate our experimental procedure. In these simulations, size polydispersity and maximum particle-to-particle separation d (representing the grafting molecule size, but also kinetic factors such as the probability to diffuse into small crevices) were taken into account. As expected, a small polydispersity (1%) already had a large influence on the average number of patches per particle: the median patch number shifted from 12 for perfectly monodisperse particles to 6 for the case of $d = 0.001\bar{\sigma}$. Fluorescent labeling enabled us to experimentally determine the number of patches/protrusions per particle in our samples in a much more facile way than by electron tomography, namely, by analyzing 3D confocal z-stacks. A particle tracking and bond order analysis algorithm was used to render the structure of the particle dispersions and extract patch number distributions and the local symmetries around each particle on which the patches formed. For a sample of core particle dispersity 1%, an average patch number of 5.0 was found (1194 counted cores). The patch number distribution was centered around 5 patches per particle, close to the prediction from simulations for a cutoff distance of $0.001\bar{\sigma}$ (distribution centered around 6 patches per particle). The angles between the protrusions agreed with the bond angles of an FCC lattice.

According to the simulations, a particle core polydispersity below 0.5% is required to approach 12 patches per particle in future studies (for silane-coupling agents in nm size range and colloids of several hundred nm in diameter). Alternatively, a cutoff distance d close to $0.1\bar{\sigma}$ may be used; however, experimentally, kinetic effects may prevent longer molecules from diffusing into the colloidal crystal. A third route to increase the number or patches could be the use of more deformable particles, such as silica shells.[105,106] Centrifugation techniques such as in refs 107−109 may be applied in future research to separate particles of different patch numbers. In a glassy system, the volume fraction and number of contacts among colloids may even be slightly higher than in a colloidal crystal,[110] so colloidal glasses could be used to increase the patch number and/or to obtain patchy particles with more than 12 patches. However, the distribution of the patches on the particles would be much more random, making it not possible to self-assemble into more regular, crystalline arrangements.

Finally, we showed that patchy silica particles with titania protrusions form gel structures in the low-polar solvents DCE and CHC. The steric stabilization provided by the SCA grafting prevents the silica surfaces/core particles from adhering to each other, leaving the possibility that the patches adhere to other patches or to the antipatch. The nature of the interparticle interactions was further investigated by mixing silica spheres, dye-labeled titania, and OTMS-grafted silica spheres separately in CHC and in DCE. We found that both types of particles are positively charged in DCE, while in CHC the OTMS-grafted silica was negatively charged and the titania positively charged. Therefore, we posit that, in CHC, protrusions adhere to the antipatch or to other protrusions due to the absence of a hydrophobic grafting and sufficient

charge stabilization, and in DCE to other protrusions only (a patch−patch interaction).

In short, we developed a system of patchy particles with protrusions that can be imaged and characterized by confocal microscopy. Toward this goal, the particles had a fluorescent dye incorporated into or selectively attached to the protrusions. The infiltration with SCA also rendered the titania protrusions stable against annealing, which may be important for applications in catalysis and active matter. We exploited the fluorescently labeled patchy particles to obtain the dispersion structure in 3D from confocal z-stacks, and to extract data on the numbers and symmetries of protrusions per particle, in this way being able study much larger numbers of particles than via electron tomography. The experimental data were compared to simulations predicting the number of contact points in a colloidal crystal as a function of core particle polydispersity p.d., and the cutoff distance for patch formation d, and showed good agreement. Finally, we illustrated in several preliminary examples that it is possible to quantitatively investigate, using confocal microscopy, the self-assembly of these patchy particles in low-polar index-matching media. Open gel-like structures were observed in several cases, where attractions between patches on the particles were present next to charge and steric repulsions between other parts of the particles of which each role in the structures being formed warrants further research. From these preliminary self-assembly studies, it is clear that a broad range of shorter and longer ranged repulsions between different parts of the particles can be present next to attractions between the patches (and possibly other parts of the particles). This allows a broad range of conditions that can be probed by exploiting differences in solvents on the charging behavior and ionic strength. It is also clear that the methodology used can be extended to amorphous packing of the particles used, giving almost identical patch numbers, but with a much less regular distribution over the particle surface, allowing the role of symmetry of the patch distribution to be investigated as well.

■ METHODS

Materials. Solvents used were ethanol (absolute, Merck), ethylene glycol (≥99.5 wt %, Fluka), acetone (pro analysis, Merck), and toluene (≥99.5 wt %, Sigma-Aldrich). Water was deionized with a Milli-Q system (Millipore Corporation) and had a resistivity of at least 18.2 MΩ cm. The catalysts aqueous ammonia (∼25 wt %) and n-butylamine (99.5 wt %) were purchased from Sigma-Aldrich. Silane coupling agents used were (3-aminopropyl)triethoxysilane (APTES, ≥98%, Sigma-Aldrich), 3-methacryloxypropyltrimethoxysilane (MPTMS, ≥98 wt %, Sigma-Aldrich, is also known as "TPM" for "3-(trimethoxysilyl)propyl methacrylate"), and octadecyl-trimethoxysilane (OTMS, 95% [85% n-isomer], ABCR GmbH & Co via Gelest, Inc.). Precursors tetraethylorthosilicate (TES, 98 wt %) and titanium(IV) butoxide (TBT, 97 wt %) were obtained from Aldrich. The dyes fluoresceine isothiocyanate (FITC, ≥90 wt % (HPLC)) and rhodamine B isothiocyanate (RITC, mixed isomers) were ordered from Sigma-Aldrich, while 7-diethylaminocoumarin-3-carboxylic acid succinimidyl ester (DEAC-SE) was purchased from Thermo Fisher. All chemicals were used as received without further purification.

Sintering for the synthesis of silica particles with silica protrusions was carried out in a Carbolite AAF ashing furnace, while a similar Carbolite oven with type 301 controller was employed to anneal patchy particles with titania protrusions. For high-power sonication (to break up and redisperse sintered colloidal crystals) we employed a Vibra-Cell ultrasonic processor (750 W) from Sonics & Materials, Inc. Syringe pumps applied in the silica protrusion growth step were from KD Scientific, models KDS-410 (single syringe pump) and KDS-200-CE (double syringe pump). IKA RH Basic stirrers were used for magnetic stirring during silica growth.

Synthesis of Silica Particles with Silica Protrusions. Fluorescently labeled silica seeds were prepared by the method introduced by Van Blaaderen and Vrij.[89,111] A nonfluorescent silica shell was grown onto the seed particles according to the continuous growth method by Giesche,[112] which is a modification of the method by Bogush et al.[113] Colloidal crystals were then prepared from the silica colloids as follows. Particles in the size range 0.20−1.1 μm and of polydispersity ≤6% were dispersed in ethanol at volume fractions 1−5%. They were allowed to sediment in a 20 mL vial with a flat bottom and form a flat, close-packed (FCC and/or HCP) crystal.[114−116] After crystal formation, the vial was opened, and the ethanol was left to evaporate at room temperature.

To pattern the particles' surfaces with MPTMS,[47] pieces of crystal were placed in a ceramic cup inside a calcination furnace. The particles were annealed at 750 °C for 5 h with 1 h heat-up and cool-down time. To coat the free surfaces of the particles, 50 mg of annealed colloidal crystal was placed into a reaction mixture of 40 mL of ethanol, 1.5 g of H_2O, 0.50 mL of silane coupling agent MPTMS, and 1.0 mL of aqueous ammonia. The mixture was left for 24 h in quiescent condition. The colloidal crystal was then washed five times with ethanol to remove nonreacted silane coupling agent. For a *double* MPTMS grafting, the crystal was dried under a stream of nitrogen and the same coating step repeated. The crystal was broken up into individual particles in ethanol using an ultrasonic processor (at 25% amplitude for 0.5 h and with pulses of 5 at 1 s intervals). Crystals larger than a few millimeters in diameter were broken up into smaller pieces with a spatula prior to sonication, as we found that such large crystals did not break up through sonication within a reasonable time span (2 h).

To grow silica protrusions onto MPTMS-patterned particles, we used the method of Wang et al.;[47] however, all volumes were 5 times smaller: to 8.0 mL of a dispersion of patterned silica particles were added 1.00 g of water and 0.20 mL of aqueous ammonia. The silica content was not adjusted for particle size, but kept at 0.50 g/L. A TES solution (8.0 μL of TES in 8.0 mL of ethanol) was added under magnetic stirring at a rate of 0.72 mL/h, using a syringe pump. For micron-sized particles, the total amount of TES solution added was increased to 16.0 mL, still added at a rate of 0.72 mL/h. In one experiment, the influence of extended protrusion growth on MPTMS-patterned particles was studied. In this study, a total volume of 24 μL of TES in 24.0 mL of ethanol was added under magnetic stirring (still at a rate of 0.72 mL/h). After 17.3 mL of precursor solution had been added, 0.30 mL of aqueous ammonia was added to compensate for the dilution of the ammonia concentration by the added TES/ethanol mixture.

We found that the annealing step can be circumvented by carrying out the grafting step in an apolar solvent such as toluene; we call this grafting method the "anhydrous" route. A dried colloidal silica crystal was not found to redisperse when placed in toluene, probably as a result of the hydrophilicity of the particle surface. We typically placed ∼20 mg of crystal in a reaction mixture[117,118] of toluene (10.0 mL), butylamine (1.0 mL), and silane coupling agent MPTMS or OTMS (1.0 mL). The butylamine acts as a catalyst, analogously to ammonia in the Stöber-like method. The colloidal crystal was left in the reaction mixture for 24 h. The crystal was washed once with toluene, and placed in an oven at 100 °C for 1 h to ensure complete condensation of the silane coupling agent with the silica surface. Two additional washing steps with toluene and three with ethanol followed. Finally, the crystal was placed in ethanol and broken up by sonication with an ultrasonic processor (0.5 h at an amplitude of 25% and with pulses of 5 at 1 s intervals).

Fluorescently Labeled Silica Protrusions. To grow silica protrusions with a fluorescent dye incorporated, either a double MPTMS grafting via a Stöber-like method or an OTMS-grafting via the "anhydrous" route was needed, in order to prevent silica growth on the antipatch region. The crystal was dried under nitrogen, weighed, and broken up into single particles by sonication in ethanol with the high-power ultrasonic processor. A dispersion of 0.50 mg/

mL surface-patterned particles in ethanol was then prepared. To the 1.5 mL dispersion we slowly added two solutions, both at a rate of 67.5 μL/min: 1.5 mL of a solution of TES and 1.5 mL of a solution of dye. The TES solution consisted of 2.0 μL/mL TES in ethanol. The dye solution was prepared using a recipe based on refs 89 and 111, by first letting 5.0 mg of APTES and 5.0 mg of FITC react in 312 μL of ethanol in the dark for 8 h, and then diluting 15.0 μL of this solution in 10.0 mL of ethanol. These two solutions were added to the reaction mixture with a syringe pump from separate syringes, and under magnetic stirring. After all TES solution and dye solution had been mixed in, the reaction mixture was left to stir for five more hours, and the particles were washed with ethanol until no coloration of the supernatant was observed.

Growth of Titania Protrusions. Titania protrusions were grown according to the method by Bae et al.[119] We prepared a solution of 200 μL of TBT in 30 mL of ethylene glycol and stirred it for 12−24 h. Dry OTMS-patterned (anhydrous route) particles (1.12 ± 0.01 μm) were dispersed in acetone at a concentration of 2 mg/mL. To 40 mL of this dispersion, we added 100 μL of water (needed for hydrolysis of the TBT). Under magnetic stirring, we then added 0.5 mL of the TBT solution. The reaction mixture was left stirring overnight, and the patchy particles were collected by centrifugation and washing with ethanol.

Fluorescent Labeling of Titania Protrusions by Infiltration with APTES−Dye Conjugates and Annealing. The titania protrusions were successfully labeled with a fluorescent dye *postsynthesis*. A solution of RITC (or FITC, or DEAC-SE) conjugated to APTES was first prepared as follows: to 20 mg of RITC (or FITC, or DEAC-SE) were added 1 g (1.27 mL) of ethanol and 20 μL of APTES, after which the solution was stirred overnight. To 10 mL of a dispersion of the silica particles with titania protrusions, 100 μL of aqueous ammonia and 40 μL of dye solution were added. The APTES-RITC (or APTES-FITC, or APTES-[DEAC-SE]) conjugate molecules can penetrate the porous titania and react with the surface OH groups, as already shown before by Demirörs et al.[96] The dispersion was shaken for 2 h. The residual dye was washed away by centrifuging and replacing the supernatant with fresh ethanol until not visibly colored with dye anymore (>3 washing steps).

Some of the final particles were annealed with the objective of converting the amorphous titania protrusions into crystalline titania. Particles were dried in a ceramic cup and placed in a calcination furnace under ambient conditions. The furnace was heated to the desired temperature (500, 900, or 1100 °C) at a heating rate of 9 °C/min. After annealing for the desired time, the furnace was left to cool by itself. The ceramic cup was placed in a beaker with 40 mL of ethanol. The beaker was placed in a sonication bath to collect the annealed particles in the form of a colloidal dispersion in ethanol.

Characterization of Particle and Protrusion Sizes by Transmission Electron Microscopy (TEM) and Electron Tomography. The shape of patchy particles was examined by transmission electron microscopy (TEM) with an FEI Tecnai 10 or Tecnai 12 microscope, at respective acceleration voltages of 100 and 120 kV. High-resolution transmission electron microscopy (HR-TEM) and selected area electron diffraction (SAED) were performed on a Tecnai 20 FEG (FEI) instrument at an acceleration voltage of 200 kV. Home-made TEM grids were used as sample holders (preparation: cf. ref 120, on G200-Cu grids by Electron Microscopy Sciences). The particles were drop-cast onto the grids and dried from ethanol. Scanning electron microscopy (SEM) images were obtained utilizing a table-top Phenom or a Nova Nanolab 600 (FEI) instrument.

Particle and patch sizes were obtained from TEM images via the software program *iTEM* (version 5.0, Olympus Soft-Imaging Solutions Corp.). As uncertainty in the particle diameter, we used the standard deviation of at least 10 diameter measurements on a single particle, while the standard deviation of measurements on different particles was used as the polydispersity. Patch widths and heights were estimated by drawing line segments tangentially and orthogonally (respectively) to the core particle through the patch projection. Each patch size measurement was averaged over at least 20

counts of different patches. The standard deviation of these measurements was used as a "polydispersity" of the patch size.

For some particles we determined the 3D shape by electron tomography (see refs 121 and 122). Electron tomography is a technique with which the 3D morphology of an object can be determined by repeated TEM imaging and sample rotations. All images are Fourier transformed and combined. The projection theorem states that the 2D Fourier transform of a 2D image is equal to a 2D slice through a 3D Fourier transform of a 3D image.[123−125] A 3D inverse Fourier transform of the combined slices therefore yields a 3D image of the particle surface. The quality of the reconstruction depends on the total range of tilt angles over which the 2D images were acquired. Here, the tilt angle ranged between −60° and +60° recorded at intervals of 1−2°.

ζ Potential Measurements. ζ potential measurements were performed on a Malvern ZetaSizer Nano ZS machine, which measures mobilities by means of laser Doppler microelectrophoresis. Since the measurements involved inorganic solvents, a Malvern "dip cell" probe and a fused glass cuvette were employed. Mobility measurements consisted of 50−100 runs at a temperature of 25 °C and a voltage of 40 V. For data acquisition, we used Malvern ZetaSizer software version 5.1.

Characterization by Confocal Microscopy. Confocal images were recorded on a Leica SP8 confocal microscope with a 100× oil immersion objective (Leica HCX Plan Apo STED Orange, designed for the purpose of STED microscopy, numerical aperture (NA) = 1.4). This confocal microscope was fitted with a white light fiber laser; the wavelengths 495 and 543 nm were selected to excite FITC and RITC dye, respectively. The microscope was equipped with two types of detectors: photomultiplier tubes (PMTs) and hybrid detectors (HyDs) developed by Leica. HyD detectors combine a traditional PMT with an avalanche photo diode (APD), resulting in a higher sensitivity and signal-to-noise ratio for these detectors. Fluorescent signals from the dyes were recorded on such HyD detectors. For imaging of particles with DEAC-SE dye, we used a similar microscope setup equipped with a 405 nm diode laser. Samples were prepared either by filling a borosilicate capillary (VitroCom no. 5010 or no. 5012, n = 1.474 at 589.3 nm) or by building a sample cell from coverslips (Menzel Gläzer, no.1) as in ref 126. The capillaries were sealed with Norland optical adhesive no. 68, which was cured under UV light (∼350 nm). Immersion oil (Leica, type F, n = 1.52) was used between the sample and the confocal lens in all confocal imaging.

Particle Tracking Routine. An iterative particle tracking procedure was used to extract particle positions from 3D datastacks. After a Gaussian smoothing, the color channels were incrementally thresholded, and the center of mass for each patch was determined using Wavemetrics 3D particle tracking implemented in *Igor Pro 8*. For each particle found, the coordinates were recorded; the local background around the patch was determined and a Gaussian shape fitted in $\{x, y, z\}$ to determine the width and amplitude of the patch intensity. Subsequently, a Gaussian spot of equal intensity and size was subtracted from the data set, and the threshold was lowered again until all patches were found. Patches and cores were paired by finding the nearest core for each patch with a distance cutoff of r_{cutoff} = 800 nm (since for sample A, r_{core} = 540 and r_{patch} = 125) to ensure that all protrusions are captured, and free-floating/nonpaired protrusions are ignored. Finally, patch number distributions are calculated, as well as for each core particle the angles between each of its patches. The coordinate file was rendered in *POV-ray* version 3.7.

Simulations of Patch Number Distributions. Monte Carlo simulations in the isothermal−isobaric ensemble (known as "NPT") were performed to investigate to what extent the obtained patch number distributions are affected by polydispersity and maximum interparticle separation (that still allows for size exclusion of the grafting molecules). Briefly, the initial configuration for each simulation was an FCC lattice with a volume fraction slightly above 0.5 and a log-normal distribution for a specific size polydispersity. The total system size was N = 2048. The configuration was then compressed until the volume fraction remained constant. Each simulation consisted of 10^5 cycles, and per cycle on average one

attempt was carried out to change the volume by $N - 1$ attempts to move a randomly chosen particle (with $N = 2048$). The particles are hard spheres (approximated by using a Yukawa potential with $\kappa\sigma \approx 1000$, where κ is the inverse Debye length and σ the average particle diameter) with a Yukawa potential and a contact energy of $k_BT = 81$. Simulations were carried out for particle polydispersities 0%, 1%, 2%, 3%, 4%, and 5%, with five independent simulations per polydispersity value. A particle (of radius R_1) was assumed to have a patch when the distance to its neighbor (of radius R_2) was smaller than $R_1 + R_2 + d$, in which d is a cutoff distance that depends on the grafting molecule size (i.e., the maximum distance between the surfaces of the particles which still excludes the grafting molecules due to their finite size). "Rattlers", i.e., particles that could still move in a cage of other particles, were not moved downward in these simulations as they would experimentally on account of gravity. Simulations were performed for three values of d: 0.1%, 1%, and 10% of the average particle diameter. The simulations returned the coordinates of the particles in the final configuration and, more importantly, histograms of the number of patches per particle (patch number distributions).

■ ASSOCIATED CONTENT

Ⓢ Supporting Information

The Supporting Information is available free of charge at https://pubs.acs.org/doi/10.1021/acs.langmuir.9b03863.

> Additional figures; additional calculations; and additional information on fluted silica rods, dye incorporation into silica protrusions, STED, PALM, titania polymorph characterization, and solvophobic interactions (PDF)
>
> Video SV1a: tilt series of a sub-micron-sized patchy silica particle with MPTMS grafting and titania protrusions (AVI)
>
> Video SV1b: tilt series of a micron-sized patchy silica particle with MPTMS grafting and titania protrusions (AVI)
>
> Video SV2: tomographic reconstruction of the patchy particle in Video SV1a (AVI)
>
> Video SV3: surface rendering of the patchy silica particle with titania protrusions in Video SV1a, as derived from the surface rendering in Video SV2 (AVI)
>
> Video SV4: confocal 3D data stack of sample A, patchy particles in dodecanol (FITC-labeled silica cores depicted in green, RITC-labeled titania protrusions in red) (AVI)
>
> Video SV5: confocal 3D data stack of patchy particles in CHC (FITC-labeled silica cores depicted in green, RITC-labeled titania protrusions in red) (AVI)
>
> Video SV6: confocal 3D data stack of patchy particles in DCE (FITC-labeled silica cores depicted in green, RITC-labeled titania protrusions in red) (AVI)
>
> Video SV7: confocal time series of silica particles and RITC-dyed titania in CHC (FITC-labeled silica cores depicted in green, RITC-labeled titania in red; 4.4× real time) (AVI)
>
> Video SV8: confocal time series of silica particles and RITC-dyed titania in DCE (FITC-labeled silica cores depicted in green, RITC-labeled titania in red; 4.4× real time) (AVI)

■ AUTHOR INFORMATION

Corresponding Authors

Marlous Kamp − *Soft Condensed Matter, Debye Institute for Nanomaterials Science, Utrecht University, 3584 CC Utrecht, The Netherlands; NanoPhotonics Centre, Department of Physics, University of Cambridge, Cambridge CB3 0HE, United Kingdom;* ⓘ orcid.org/0000-0003-4915-1312; Email: mkamp@cantab.net

Alfons van Blaaderen − *Soft Condensed Matter, Debye Institute for Nanomaterials Science, Utrecht University, 3584 CC Utrecht, The Netherlands;* Email: A.vanBlaaderen@uu.nl

Authors

Bart de Nijs − *Soft Condensed Matter, Debye Institute for Nanomaterials Science, Utrecht University, 3584 CC Utrecht, The Netherlands; NanoPhotonics Centre, Department of Physics, University of Cambridge, Cambridge CB3 0HE, United Kingdom*

Marjolein N. van der Linden − *Soft Condensed Matter, Debye Institute for Nanomaterials Science, Utrecht University, 3584 CC Utrecht, The Netherlands*

Isja de Feijter − *Laboratory of Self-Organizing Soft Matter, Laboratory of Macromolecular and Organic Chemistry, Department of Chemical Engineering and Chemistry, Institute for Complex Molecular Systems, Eindhoven University of Technology, 5600 MB Eindhoven, The Netherlands*

Merel J. Lefferts − *Soft Condensed Matter, Debye Institute for Nanomaterials Science, Utrecht University, 3584 CC Utrecht, The Netherlands;* ⓘ orcid.org/0000-0002-5825-4500

Antonio Aloi − *Laboratory of Self-Organizing Soft Matter, Laboratory of Macromolecular and Organic Chemistry, Department of Chemical Engineering and Chemistry, Institute for Complex Molecular Systems, Eindhoven University of Technology, 5600 MB Eindhoven, The Netherlands*

Jack Griffiths − *NanoPhotonics Centre, Department of Physics, University of Cambridge, Cambridge CB3 0HE, United Kingdom*

Jeremy J. Baumberg − *NanoPhotonics Centre, Department of Physics, University of Cambridge, Cambridge CB3 0HE, United Kingdom;* ⓘ orcid.org/0000-0002-9606-9488

Ilja K. Voets − *Laboratory of Self-Organizing Soft Matter, Laboratory of Macromolecular and Organic Chemistry, Department of Chemical Engineering and Chemistry, Institute for Complex Molecular Systems, Eindhoven University of Technology, 5600 MB Eindhoven, The Netherlands;* ⓘ orcid.org/0000-0003-3543-4821

Complete contact information is available at:
https://pubs.acs.org/10.1021/acs.langmuir.9b03863

Author Contributions

M.K. performed all experimental work (except PALM modification), initiated collaborations, and wrote the manuscript. B.d.N. performed the TEM tomography reconstructions and wrote the algorithm for particle tracking and extracting patch number distributions. M.N.v.d.L. performed the simulations for theoretical patch number distributions. I.d.F. performed functionalization with Cage 552, and I.d.F. and A.A. performed PALM measurements. M.J.L. synthesized micron-sized patchy silica particles with silica protrusions under the supervision of M.K. J.G. helped to carry out particle tracking. A.v.B. designed research. I.K.V., J.J.B., and A.v.B. supervised the research. The manuscript was approved by all authors.

Notes

The authors declare no competing financial interest.

■ ACKNOWLEDGMENTS

■ REFERENCES

(1) Kraft, D. J.; Hilhorst, J.; Heinen, M. A. P.; Hoogenraad, M. J.; Luigjes, B.; Kegel, W. K. Patchy Polymer Colloids with Tunable Anisotropy Dimensions. *J. Phys. Chem. B* 2011, *115*, 7175−7181.

(2) Kraft, D. J.; Ni, R.; Smallenburg, F.; Hermes, M.; Yoon, K.; Weitz, D. A.; van Blaaderen, A.; Groenewold, J.; Dijkstra, M.; Kegel, W. K. Surface roughness directed self-assembly of patchy particles into colloidal micelles. *Proc. Natl. Acad. Sci. U. S. A.* 2012, *109*, 10787−10792.

(3) Bianchi, E.; Kahl, G.; Likos, C. N.; Sciortino, F. Patchy particles. *J. Phys.: Condens. Matter* 2015, *27*, 230301.

(4) Wang, Y.; Wang, Y.; Breed, D. R.; Manoharan, V. N.; Feng, L.; Hollingsworth, A. D.; Weck, M.; Pine, D. J. Colloids with valence and specific directional bonding. *Nature* 2012, *491*, 51−55.

(5) van Blaaderen, A. Materials Science: Colloids get complex. *Nature* 2006, *439*, 545−546.

(6) Sacanna, S.; Korpics, M.; Rodriguez, K.; Colón-Meléndez, L.; Kim, S.-H.; Pine, D. J.; Yi, G.-R. Shaping colloids for self-assembly. *Nat. Commun.* 2013, *4*, 1688.

(7) Lunn, D. J.; Finnegan, J. R.; Manners, I. Self-assembly of "patchy" nanoparticles: a versatile approach to functional hierarchical materials. *Chemical Science* 2015, *6*, 3663−3673.

(8) Kumar, A.; Park, B. J.; Tu, F.; Lee, D. Amphiphilic Janus particles at fluid interfaces. *Soft Matter* 2013, *9*, 6604−6617.

(9) Yi, G.-R.; Pine, D. J.; Sacanna, S. Recent progress on patchy colloids and their self-assembly. *J. Phys.: Condens. Matter* 2013, *25*, 193101.

(10) Walther, A.; Müller, A. H. E. Janus Particles: Synthesis, Self-Assembly, Physical Properties, and Applications. *Chem. Rev.* 2013, *113*, 5194−5261.

(11) Kaewsaneha, C.; Tangboriboonrat, P.; Polpanich, D.; Eissa, M.; Elaissari, A. Janus Colloidal Particles: Preparation, Properties, and Biomedical Applications. *ACS Appl. Mater. Interfaces* 2013, *5*, 1857−1869.

(12) Song, Y.; Chen, S. Janus Nanoparticles: Preparation, Characterization, and Applications. *Chem. - Asian J.* 2014, *9*, 418−430.

(13) Duguet, E.; Hubert, C.; Chomette, C.; Perro, A.; Ravaine, S. Patchy colloidal particles for programmed self-assembly. *C. R. Chim.* 2016, *19*, 173−182.

(14) Elacqua, E.; Zheng, X.; Shillingford, C.; Liu, M.; Weck, M. Molecular Recognition in the Colloidal World. *Acc. Chem. Res.* 2017, *50*, 2756−2766.

(15) Bianchi, E.; van Oostrum, P. D.; Likos, C. N.; Kahl, G. Inverse patchy colloids: Synthesis, modeling and self-organization. *Curr. Opin. Colloid Interface Sci.* 2017, *30*, 8−15.

(16) Teixeira, P.; Tavares, J. Phase behaviour of pure and mixed patchy colloids − Theory and simulation. *Curr. Opin. Colloid Interface Sci.* 2017, *30*, 16−24.

(17) Bradley, L. C.; Chen, W.-H.; Stebe, K. J.; Lee, D. Janus and patchy colloids at fluid interfaces. *Curr. Opin. Colloid Interface Sci.* 2017, *30*, 25−33.

(18) Porter, C. L.; Crocker, J. C. Directed assembly of particles using directional DNA interactions. *Curr. Opin. Colloid Interface Sci.* 2017, *30*, 34−44.

(19) Ravaine, S.; Duguet, E. Synthesis and assembly of patchy particles: Recent progress and future prospects. *Curr. Opin. Colloid Interface Sci.* 2017, *30*, 45−53.

(20) Petukhov, A. V.; Tuinier, R.; Vroege, G. J. Entropic patchiness: Effects of colloid shape and depletion. *Curr. Opin. Colloid Interface Sci.* 2017, *30*, 54−61.

(21) Avendaño, C.; Escobedo, F. A. Packing, entropic patchiness, and self-assembly of non-convex colloidal particles: A simulation perspective. *Curr. Opin. Colloid Interface Sci.* 2017, *30*, 62−69.

(22) Morphew, D.; Chakrabarti, D. Clusters of anisotropic colloidal particles: From colloidal molecules to supracolloidal structures. *Curr. Opin. Colloid Interface Sci.* 2017, *30*, 70−80.

(23) Aubret, A.; Ramananarivo, S.; Palacci, J. Eppur si muove, and yet it moves: Patchy (phoretic) swimmers. *Curr. Opin. Colloid Interface Sci.* 2017, *30*, 81−89.

(24) Jiang, S.; Van Dyk, A.; Maurice, A.; Bohling, J.; Fasano, D.; Brownell, S. Design colloidal particle morphology and self-assembly for coating applications. *Chem. Soc. Rev.* 2017, *46*, 3792−3807.

(25) Sciortino, F.; Zaccarelli, E. Equilibrium gels of limited valence colloids. *Curr. Opin. Colloid Interface Sci.* 2017, *30*, 90−96.

(26) Jo, I.-S.; Lee, S.; Zhu, J.; Shim, T. S.; Yi, G.-R. Soft patchy micelles. *Curr. Opin. Colloid Interface Sci.* 2017, *30*, 97−105.

(27) Evers, C. H.; Luiken, J. A.; Bolhuis, P. G.; Kegel, W. K. Self-assembly of microcapsules via colloidal bond hybridization and anisotropy. *Nature* 2016, *534*, 364−368.

(28) Bianchi, E.; Largo, J.; Tartaglia, P.; Zaccarelli, E.; Sciortino, F. Phase Diagram of Patchy Colloids: Towards Empty Liquids. *Phys. Rev. Lett.* 2006, *97*, 168301.

(29) Chen, Q.; Bae, S. C.; Granick, S. Directed self-assembly of a colloidal kagome lattice. *Nature* 2011, *469*, 381−384.

(30) Chen, Q.; Whitmer, J. K.; Jiang, S.; Bae, S. C.; Luijten, E.; Granick, S. Supracolloidal Reaction Kinetics of Janus Spheres. *Science* 2011, *331*, 199−202.

(31) Morgan, J. W. R.; Chakrabarti, D.; Dorsaz, N.; Wales, D. J. Designing a Bernal Spiral from Patchy Colloids. *ACS Nano* 2013, *7*, 1246−1256.

(32) Munaò, G.; Preisler, Z.; Vissers, T.; Smallenburg, F.; Sciortino, F. Cluster formation in one-patch colloids: low coverage results. *Soft Matter* 2013, *9*, 2652−2661.

(33) Preisler, Z.; Vissers, T.; Smallenburg, F.; Munaò, G.; Sciortino, F. Phase Diagram of One-Patch Colloids Forming Tubes and Lamellae. *J. Phys. Chem. B* 2013, *117*, 9540−9547.

(34) Munaò, G.; O'Toole, P.; Hudson, T. S.; Costa, D.; Caccamo, C.; Giacometti, A.; Sciortino, F. Phase separation and self-assembly of colloidal dimers with tunable attractive strength: from symmetrical square-wells to Janus dumbbells. *Soft Matter* 2014, *10*, 5269−5279.

(35) Preisler, Z.; Vissers, T.; Munaò, G.; Smallenburg, F.; Sciortino, F. Equilibrium phases of one-patch colloids with short-range attractions. *Soft Matter* **2014**, *10*, 5121−5128.

(36) Guo, R.; Mao, J.; Xie, X.-M.; Yan, L.-T. Predictive supracolloidal helices from patchy particles. *Sci. Rep.* **2015**, *4*, 7021.

(37) Vissers, T.; Smallenburg, F.; Munaò, G.; Preisler, Z.; Sciortino, F. Cooperative polymerization of one-patch colloids. *J. Chem. Phys.* **2014**, *140*, 144902.

(38) Munaò, G.; O'Toole, P.; Hudson, T. S.; Costa, D.; Caccamo, C.; Sciortino, F.; Giacometti, A. Cluster formation and phase separation in heteronuclear Janus dumbbells. *J. Phys.: Condens. Matter* **2015**, *27*, 234101.

(39) Wolters, J. R.; Avvisati, G.; Hagemans, F.; Vissers, T.; Kraft, D. J.; Dijkstra, M.; Kegel, W. K. Self-assembly of "Mickey Mouse" shaped colloids into tube-like structures: experiments and simulations. *Soft Matter* **2015**, *11*, 1067−1077.

(40) Wolters, J. R.; Verweij, J. E.; Avvisati, G.; Dijkstra, M.; Kegel, W. K. Depletion-Induced Encapsulation by Dumbbell-Shaped Patchy Colloids Stabilize Microspheres against Aggregation. *Langmuir* **2017**, *33*, 3270−3280.

(41) Munaò, G.; Costa, D.; Prestipino, S.; Caccamo, C. Aggregation of colloidal spheres mediated by Janus dimers: A Monte Carlo study. *Colloids Surf., A* **2017**, *532*, 397−404.

(42) Chaudhary, K.; Juareza, J. J.; Chen, Q.; Granick, S.; Lewis, J. A. Reconfigurable assemblies of Janus rods in AC electric fields. *Soft Matter* **2014**, *10*, 1320−1324.

(43) Shah, A. A.; Schultz, B.; Zhang, W.; Glotzer, S. C.; Solomon, M. J. Actuation of shape-memory colloidal fibres of Janus ellipsoids. *Nat. Mater.* **2015**, *14*, 117−124.

(44) Zhao, B.; Zhou, H.; Liu, C.; Long, Y.; Yang, G.; Tung, C.-H.; Song, K. Fabrication and directed assembly of magnetic Janus rods. *New J. Chem.* **2016**, *40*, 6541−6545.

(45) Yan, J.; Chaudhary, K.; Chul Bae, S.; Lewis, J. A.; Granick, S. Colloidal ribbons and rings from Janus magnetic rods. *Nat. Commun.* **2013**, *4*, 1516.

(46) Fan, W.; Liu, L.; Zhao, H. Co-assembly of patchy polymeric micelles and protein molecules. *Angew. Chem., Int. Ed.* **2017**, *56*, 8844−8848.

(47) Wang, L.; Xia, L.; Li, G.; Ravaine, S.; Zhao, X.-S. Patterning the Surface of Colloidal Microspheres and Fabrication of Nonspherical Particles. *Angew. Chem., Int. Ed.* **2008**, *47*, 4725−4728.

(48) Bae, C.; Kim, H.; Moreno, J. M. M.; Yi, G.-R.; Shin, H. Toward Coordinated Colloids: Site-Selective Growth of Titania on Patchy Silica Particles. *Sci. Rep.* **2015**, *5*, 9339.

(49) Wang, Y.; Wang, Y.; Zheng, X.; Ducrot, É.; Yodh, J. S.; Weck, M.; Pine, D. J. Crystallization of DNA-coated colloids. *Nat. Commun.* **2015**, *6*, 7253.

(50) Jiang, K.; Liu, Y.; Yan, Y.; Wang, S.; Liu, L.; Yang, W. Combined chain- and step-growth dispersion polymerization toward PSt particles with soft, clickable patches. *Polym. Chem.* **2017**, *8*, 1404−1416.

(51) Yan, W.; Pan, M.; Yuan, J.; Liu, G.; Cui, L.; Zhang, G.; Zhu, L. Raspberry-like patchy particles achieved by decorating carboxylated polystyrene cores with snowman-like poly(vinylidene fluoride)/ poly(4-vinylpyridiene) Janus particles. *Polymer* **2017**, *122*, 139−147.

(52) Gong, Z.; Hueckel, T.; Yi, G.-R.; Sacanna, S. Patchy particles made by colloidal fusion. *Nature* **2017**, *550*, 234−238.

(53) Mihut, A. M.; Stenqvist, B.; Lund, M.; Schurtenberger, P.; Crassous, J. J. Assembling oppositely charged lock and key responsive colloids: A mesoscale analog of adaptive chemistry. *Science Advances* **2017**, *3*, e1700321.

(54) Curk, T.; Dobnikar, J.; Frenkel, D. *Multivalency*; John Wiley and Sons, Ltd, 2017; Chapter 3, pp 75−101.

(55) Benyettou, F.; Zheng, X.; Elacqua, E.; Wang, Y.; Dalvand, P.; Asfari, Z.; Olsen, J.-C.; Han, D. S.; Saleh, N.; Elhabiri, M.; Weck, M.; Trabolsi, A. Redox-Responsive Viologen-Mediated Self-Assembly of CB[7]-Modified Patchy Particles. *Langmuir* **2016**, *32*, 7144−7150.

(56) Elacqua, E.; Zheng, X.; Weck, M. Light-Mediated Reversible Assembly of Polymeric Colloids. *ACS Macro Lett.* **2017**, *6*, 1060−1065.

(57) Jang, S.; Kim, K.; Jeon, J.; Kang, D.; Sohn, B.-H. Supracolloidal chains of patchy micelles of diblock copolymers with in situ synthesized nanoparticles. *Soft Matter* **2017**, *13*, 6756−6760.

(58) Nguyen, T. A.; Newton, A.; Kraft, D. J.; Bolhuis, P. G.; Schall, P. Tuning Patchy Bonds Induced by Critical Casimir Forces. *Materials* **2017**, *10*, 1265.

(59) Zheng, X.; Liu, M.; He, M.; Pine, D. J.; Weck, M. Shape-Shifting Patchy Particles. *Angew. Chem.* **2017**, *129*, 5599−5603.

(60) Bradley, L. C.; Stebe, K. J.; Lee, D. Clickable Janus Particles. *J. Am. Chem. Soc.* **2016**, *138*, 11437−11440.

(61) Dias, C. S.; Tavares, J. M.; Araújo, N. A. M.; da Gama, M. M. T. Temperature driven dynamical arrest of a network fluid: the role of loops. 2016, arXiv:1604.05279v1. arXiv.org e-Print archive. https://arxiv.org/abs/1604.05279v1.

(62) Zaccarelli, E. Colloidal gels: equilibrium and non-equilibrium routes. *J. Phys.: Condens. Matter* **2007**, *19*, 323101.

(63) Tavares, J. M.; Dias, C. S.; Araújo, N. A. M.; Telo da Gama, M. M. Dynamics of Patchy Particles in and out of Equilibrium. *J. Phys. Chem. B* **2018**, *122*, 3514−3518.

(64) Dias, C. a. S.; Araújo, N. A. M.; Telo da Gama, M. M. Non-equilibrium adsorption of 2A*n*B patchy colloids on substrates. *Soft Matter* **2013**, *9*, 5616−5623.

(65) Dias, C. S.; Araújo, N. A. M.; Telo da Gama, M. M. Nonequilibrium growth of patchy-colloid networks on substrates. *Phys. Rev. E* **2013**, *87*, 032308.

(66) Dias, C.; Araújo, N.; da Gama, M. T. Effect of the number of patches on the growth of networks of patchy colloids on substrates. *Mol. Phys.* **2015**, *113*, 1069−1075.

(67) Tito, N.; Frenkel, D. Switch-like surface binding of competing multivalent particles. *Eur. Phys. J.: Spec. Top.* **2016**, *225*, 1673−1682.

(68) Reinhardt, A.; Ho, C. P.; Frenkel, D. Effects of co-ordination number on the nucleation behaviour in many-component self-assembly. *Faraday Discuss.* **2016**, *186*, 215−228.

(69) Newton, A. C.; Groenewold, J.; Kegel, W. K.; Bolhuis, P. G. The role of multivalency in the association kinetics of patchy particle complexes. *J. Chem. Phys.* **2017**, *146*, 234901.

(70) Sciortino, F. Gel-forming patchy colloids and network glass formers: thermodynamic and dynamic analogies. *Eur. Phys. J. B* **2008**, *64*, 505−509.

(71) Russo, J.; Tartaglia, P.; Sciortino, F. Reversible gels of patchy particles: Role of the valence. *J. Chem. Phys.* **2009**, *131*, 014504.

(72) Sciortino, F.; Zaccarelli, E. Reversible gels of patchy particles. *Curr. Opin. Solid State Mater. Sci.* **2011**, *15*, 246−253.

(73) Wang, G.; Swan, J. W. Surface heterogeneity affects percolation and gelation of colloids: dynamic simulations with random patchy spheres. *Soft Matter* **2019**, *15*, 5094−5108.

(74) Ruzicka, B.; Zaccarelli, E.; Zulian, L.; Angelini, R.; Sztucki, M.; Moussaïd, A.; Narayanan, T.; Sciortino, F. Observation of empty liquids and equilibrium gels in a colloidal clay. *Nat. Mater.* **2011**, *10*, 56−60.

(75) Bianchi, E.; Kahl, G.; Likos, C. N. Inverse patchy colloids: from microscopic description to mesoscopic coarse-graining. *Soft Matter* **2011**, *7*, 8313−8323.

(76) Stipsitz, M.; Kahl, G.; Bianchi, E. Generalized inverse patchy colloid model. *J. Chem. Phys.* **2015**, *143*, 114905.

(77) Ferrari, S.; Bianchi, E.; Kalyuzhnyi, Y. V.; Kahl, G. Inverse patchy colloids with small patches: fluid structure and dynamical slowing down. *J. Phys.: Condens. Matter* **2015**, *27*, 234104.

(78) van Oostrum, P. D. J.; Hejazifar, M.; Niedermayer, C.; Reimhult, E. Simple method for the synthesis of inverse patchy colloids. *J. Phys.: Condens. Matter* **2015**, *27*, 234105.

(79) Sabapathy, M.; Ann Mathews K, R.; Mani, E. Self-assembly of inverse patchy colloids with tunable patch coverage. *Phys. Chem. Chem. Phys.* **2017**, *19*, 13122−13132.

(80) Bernal, J. D.; Mason, J. Packing of Spheres: Co-ordination of Randomly Packed Spheres. *Nature* **1960**, *188*, 910−911.

(81) van Blaaderen, A.; Wiltzius, P. Template-directed colloidal crystallization. *Science* **1995**, *270*, 1177−1179.

(82) Midgley, P. A.; Dunin-Borkowski, R. E. Electron tomography and holography in materials science. *Nat. Mater.* **2009**, *8*, 271−280.

(83) Pronk, S.; Frenkel, D. Point defects in hard-sphere crystals. *J. Phys. Chem. B* **2001**, *105*, 6722−6727.

(84) Kuijk, A.; van Blaaderen, A.; Imhof, A. Synthesis of Monodisperse, Rodlike Silica Colloids with Tunable Aspect Ratio. *J. Am. Chem. Soc.* **2011**, *133*, 2346−2349.

(85) Peng, B.; Soligno, G.; Kamp, M.; de Nijs, B.; de Graaf, J.; Dijkstra, M.; van Roij, R.; van Blaaderen, A.; Imhof, A. Site-specific growth of polymers on silica rods. *Soft Matter* **2014**, *10*, 9644−9650.

(86) Míguez, H.; Meseguer, F.; López, C.; Blanco, A.; Moya, J. S.; Requena, J.; Mifsud, A.; Fornés, V. Control of the Photonic Crystal Properties of fcc-Packed Submicrometer SiO₂ Spheres by Sintering. *Adv. Mater.* **1998**, *10*, 480−483.

(87) Chabanov, A. A.; Jun, Y.; Norris, D. J. Avoiding cracks in self-assembled photonic band-gap crystals. *Appl. Phys. Lett.* **2004**, *84*, 3573−3575.

(88) Shrivastava, V. P.; Kumar, J.; Sivakumar, S. On the controlled isotropic shrinkage induced fine-tuning of photo-luminescence in terbium ions embedded silica inverse opal films. *AIP Adv.* **2017**, *7*, 125027.

(89) Van Blaaderen, A.; Vrij, A. Synthesis and characterization of colloidal dispersions of fluorescent, monodisperse silica spheres. *Langmuir* **1992**, *8*, 2921−2931.

(90) Mačković, M.; Niekiel, F.; Wondraczek, L.; Spiecker, E. Direct observation of electron-beam-induced densification and hardening of silica nanoballs by in situ transmission electron microscopy and finite element method simulations. *Acta Mater.* **2014**, *79*, 363−373.

(91) Mačković, M.; Niekiel, F.; Wondraczek, L.; Bitzek, E.; Spiecker, E. In situ mechanical quenching of nanoscale silica spheres in the transmission electron microscope. *Scr. Mater.* **2016**, *121*, 70−74.

(92) Demirörs, A. F.; van Blaaderen, A.; Imhof, A. Synthesis of Eccentric Titania-Silica Core-Shell and Composite Particles. *Chem. Mater.* **2009**, *21*, 979−984.

(93) Lawrie, G.; Grøndahl, L.; Battersby, B.; Keen, I.; Lorentzen, M.; Surawski, P.; Trau, M. Tailoring Surface Properties To Build Colloidal Diagnostic Devices: Controlling Interparticle Associations. *Langmuir* **2006**, *22*, 497−505.

(94) de Feijter, I.; Albertazzi, L.; Palmans, A. R.; Voets, I. K. Stimuli-Responsive Colloidal Assembly Driven by Surface-Grafted Supramolecular Moieties. *Langmuir* **2015**, *31*, 57−64.

(95) Vilanova, N.; de Feijter, I.; Teunissen, A. J. P.; Voets, I. K. Light induced assembly and self-sorting of silica microparticles. *Sci. Rep.* **2018**, *8*, 1271.

(96) Demirörs, A. F.; van Blaaderen, A.; Imhof, A. A General Method to Coat Colloidal Particles with Titania. *Langmuir* **2010**, *26*, 9297−9303.

(97) Panwar, K.; Jassal, M.; Agrawal, A. K. TiO₂−SiO₂ Janus particles with highly enhanced photocatalytic activity. *RSC Adv.* **2016**, *6*, 92754−92764.

(98) Palacci, J.; Sacanna, S.; Kim, S.-H.; Yi, G.-R.; Pine, D. J.; Chaikin, P. M. Light-activated self-propelled colloids. *Philos. Trans. R. Soc., A* **2014**, *372*, 20130372.

(99) Weast, R. *Handbook of Chemistry & Physics*, 65th ed.; CRC Press, 1984.

(100) Brinker, C. Hydrolysis and condensation of silicates: Effects on structure. *J. Non-Cryst. Solids* **1988**, *100*, 31−50.

(101) Harris, M. T.; Brunson, R. R.; Byers, C. H. The base-catalyzed hydrolysis and condensation reactions of dilute and concentrated TES solutions. *J. Non-Cryst. Solids* **1990**, *121*, 397−403.

(102) Bogush, G.; Zukoski IV, C. Studies of the kinetics of the precipitation of uniform silica particles through the hydrolysis and condensation of silicon alkoxides. *J. Colloid Interface Sci.* **1991**, *142*, 1−18.

(103) Liu, B.; Besseling, T. H.; Hermes, M.; Demirörs, A. F.; Imhof, A.; van Blaaderen, A. Switching plastic crystals of colloidal rods with electric fields. *Nat. Commun.* **2014**, *5*, 3092.

(104) Vlug, W. S. *Balls, beams and blocks: In situ observation of colloidal particles in confinement and under electron irradiation*; Utrecht University, 2017.

(105) Kamp, M.; Elbers, N. A.; Troppenz, T.; Imhof, A.; Dijkstra, M.; van Roij, R.; van Blaaderen, A. Electric-Field-Induced Lock-and-Key Interactions between Colloidal Spheres and Bowls. *Chem. Mater.* **2016**, *28*, 1040−1048.

(106) Elbers, N. A.; Jose, J.; Imhof, A.; van Blaaderen, A. Bulk Scale Synthesis of Monodisperse PDMS Droplets above three micrometer and Their Encapsulation by Elastic Shells. *Chem. Mater.* **2015**, *27*, 1709−1719.

(107) Kraft, D. J.; Vlug, W. S.; van Kats, C. M.; van Blaaderen, A.; Imhof, A.; Kegel, W. K. Self-Assembly of Colloids with Liquid Protrusions. *J. Am. Chem. Soc.* **2009**, *131*, 1182−1186.

(108) Cho, Y.-S.; Yi, G.-R.; Kim, S.-H.; Elsesser, M. T.; Breed, D. R.; Yang, S.-M. Homogeneous and heterogeneous binary colloidal clusters formed by evaporation-induced self-assembly inside droplets. *J. Colloid Interface Sci.* **2008**, *318*, 124−133.

(109) Qiu, P.; Mao, C. Viscosity Gradient as a Novel Mechanism for the Centrifugation-Based Separation of Nanoparticles. *Adv. Mater.* **2011**, *23*, 4880−4885.

(110) van der Linden, M. N.; El Masri, D.; Dijkstra, M.; van Blaaderen, A. Expansion of charged colloids after centrifugation: formation and crystallisation of long-range repulsive glasses. *Soft Matter* **2013**, *9*, 11618−11633.

(111) Verhaegh, N. A. M.; Blaaderen, A. v. Dispersions of rhodamine-labeled silica spheres: synthesis, Characterization, and Fluorescence Confocal Scanning Laser Microscopy. *Langmuir* **1994**, *10*, 1427−1438.

(112) Giesche, H. Synthesis of monodispersed silica powders II. Controlled growth reaction and continuous production process. *J. Eur. Ceram. Soc.* **1994**, *14*, 205−214.

(113) Bogush, G.; Tracy, M.; Zukoski IV, C. Preparation of monodisperse silica particles: Control of size and mass fraction. *J. Non-Cryst. Solids* **1988**, *104*, 95−106.

(114) Petukhov, A. V.; Thijssen, J. H. J.; Imhof, A.; van Blaaderen, A.; Dolbnya, I. P.; Snigirev, A.; Snigireva, I.; Drakopoulos, M. 3D structure and dis-(order) in photonic crystals by microradian synchrotron X-ray diffraction. *ESRF Newsletter* **2003**, *38*, 19−20.

(115) Thijssen, J. H. J.; Petukhov, A. V.; 't Hart, D. C.; Imhof, A.; van der Werf, C. H. M.; Schropp, R. E. I.; van Blaaderen, A. Characterization of Photonic Colloidal Single Crystals by Microradian X-ray Diffraction. *Adv. Mater.* **2006**, *18*, 1662−1666.

(116) Petukhov, A. V.; Thijssen, J. H. J.; 't Hart, D. C.; Imhof, A.; van Blaaderen, A.; Dolbnya, I. P.; Snigirev, A.; Moussaïd, A.; Snigireva, I. Microradian X-ray diffraction in colloidal photonic crystals. *J. Appl. Crystallogr.* **2006**, *39*, 137−144.

(117) Mooney, J. F.; Hunt, A. J.; McIntosh, J. R.; Liberko, C. A.; Walba, D.; Rogers, C. Patterning of functional antibodies and other proteins by photolithography of silane monolayers. *Proc. Natl. Acad. Sci. U. S. A.* **1996**, *93*, 12287−12291.

(118) Vogel, B. M.; DeLongchamp, D. M.; Mahoney, C. M.; Lucas, L. A.; Fischer, D. A.; Lin, E. K. Interfacial modification of silica surfaces through γ-isocyanatopropyl triethoxy silane-amine coupling reactions. *Appl. Surf. Sci.* **2008**, *254*, 1789−1796.

(119) Bae, C.; Moon, J.; Shin, H.; Kim, J.; Sung, M. M. Fabrication of Monodisperse Asymmetric Colloidal Clusters by Using Contact Area Lithography (CAL). *J. Am. Chem. Soc.* **2007**, *129*, 14232−14239.

(120) Bozzola, J. J.; Russell, L. D. *Electron Microscopy: Principles and Techniques for Biologists*; Jones and Bartlett Publishers, Inc., 1999.

(121) Friedrich, H.; Gommes, C. J.; Overgaag, K.; Meeldijk, J. D.; Evers, W. H.; de Nijs, B.; Boneschanscher, M. P.; de Jongh, P. E.; Verkleij, A. J.; de Jong, K. P.; van Blaaderen, A.; Vanmaekelbergh, D. Quantitative Structural Analysis of Binary Nanocrystal Superlattices by Electron Tomography. *Nano Lett.* **2009**, *9*, 2719−2724.

(122) de Nijs, B.; Dussi, S.; Smallenburg, F.; Meeldijk, J. D.; Groenendijk, D. J.; Filion, L.; Imhof, A.; van Blaaderen, A.; Dijkstra, M. Entropy-driven formation of large icosahedral colloidal clusters by spherical confinement. *Nat. Mater.* **2015**, *14*, 56−60.

(123) Durrani, T.; Bisset, D. The Radon transform and its properties. *Geophysics* **1984**, *49*, 1180−1187.

(124) Radermacher, M. Three-dimensional reconstruction from random projections: orientational alignment via Radon transforms. *Ultramicroscopy* **1994**, *53*, 121−136.

(125) Natterer, F. *The Mathematics of Computerized Tomography*; Vieweg+Teubner Verlag, 1986.

(126) Besseling, T.; Jose, J.; van Blaaderen, A. Methods to calibrate and scale axial distances in confocal microscopy as a function of refractive index. *J. Microsc.* **2015**, *257*, 142−150.